Estimating anelastic dispersion from uncorrelated vibe data

Kris Innanen

ABSTRACT

A vibroseis sweep and a dispersive geological volume act to negate each other: the sweep delays the arrival of higher frequencies and the dispersive medium hurries them along. We derive a simple analysis procedure in which the time-frequency spectra of a programmed sweep and an uncorrelated measurement of that signal after propagation are compared in order to estimate the frequency-dependence of the phase velocity. The approach is developed with a synthetic example and applied to a 3C VSP data set. Geophysically reasonable phase velocity estimates — though ones which must still be independently verified — are derived.

INTRODUCTION

In a sense, vibroseis sweeps and anelastic/dispersive Earth volumes counteract one another. The sweep causes higher seismic frequencies to arrive later at a geophone, and the dispersive volume causes them to arrive sooner. The purpose of this paper is to explore some of the consequences of this, both in an applied sense, wherein we use this fact to estimate the dispersive seismic phase velocity one frequency at a time, and in a more philosophical sense, wherein we imagine some strange but physically realizable pathological examples of it in action.

From an applied perspective, what sets this approach apart in the panoply of dispersion estimation methods (in which we include all Q estimation, e.g., Tonn, 1991; Zhang and Ulrych, 2002; Cheng, 2013) is that it allows each phase velocity, i.e., the value $c(f)$ for any given frequency f, to be determined individually. Normally during Q estimation a single value of Q is inferred, and only then through an assumed Q model and reference velocity, for instance

$$c(f) = c_{\text{ref}} \left[1 - \frac{1}{\pi Q} \log \left(\frac{f}{f_{\text{ref}}} \right) \right], \tag{1}$$

are the phase velocities $c(f)$, in parameterized form, subsequently determined. However it is reasonable to question whether we know with enough certainty that this Q model holds in a given volume of Earth. With the current approach $c(f)$ is observed, not inferred.

In this paper we derive and provide early synthetic and field testing of the $c(f)$ estimation. After some qualitative comments on the approach, we begin by taking the vibe sweep and dispersive wave propagation formulas, turning them into expressions that allow us to compare the departure and arrival times (at the source and receiver respectively) of particular seismic frequencies. This leads immediately to a data analysis formula giving us $c(f)$ from measured direct arrivals in a VSP experiment, assuming access to a stable time-frequency decomposition methodology. The Gabor transform (e.g., Margrave, 1998; Margrave and Lamoureux, 2001) tool in the CREWES toolbox is used in this paper.

The idea is tested with synthetic VSP data generated using a pseudo-2D Helmholtz

solver which can implement any desired body wave dispersion model. A large scale VSP experiment is synthesized and the dispersive wave velocity from a nearly constant Q model (e.g., Aki and Richards, 2002) is determined very accurately over the full synthetic bandwidth.

A walkaway 3C-VSP data set is currently being analyzed to determine Q_P and Q_S profiles. The significant attenuation and clear down-going P and S modes in this data set make it a good candidate to validate the uncorrelated data idea. The challenge in moving this idea to field data application lies primarily in the small differences between departure and arrival times; nevertheless a real signal is detected and from it we infer a phase velocity distribution with geophysically reasonable values. Independent Q analysis of the field data is ongoing (Montano et al., 2014), and this is expected to provide a benchmark against which our derived $c(f)$ can be verified.

ANALYSIS OF UNCORRELATED VIBE DATA

Qualitative remarks

In most models of body wave dispersion (Aki and Richards, 2002), high seismic frequencies propagate more quickly than low frequencies. In the standard nearly-constant Q model, and other macroscopic models based on the Kramers-Krönig relations, this is connected to imposition of causality constraints. Meanwhile, in a vibroseis sweep, though there is a tremendous freedom in determining the rate at which it happens, the low frequencies are sent into the medium before the high, and thus have a significant head start.

Consequently, a vibroseis sweep in a dispersive medium is a little like Achilles and the tortoise—the high frequencies will be using their higher phase velocities to try to catch up with the low frequencies, which will have been given a significant head start. In a standard seismic experiment and sweep (like the walkaway VSP illustrated in Figure 1) they will never manage it, since the delay in the vibe sweep is too large. The small degree to which they *do* catch up can nevertheless be measured, and used to infer the frequency dependence of the phase velocity in the medium.

We can also, though with less practical outcomes in mind, consider the type of sweep, scale of experiment, source and receiver separation, and dispersion law needed for a very interesting thing to happen — for all the frequencies delayed by the sweep to arrive at the geophone at the same time. For this special situation, the Earth will have acted as the correlator.

For the remainder of this section, we will take the standard quantities associated with vibroseis data and anelastic/dispersive wave propagation, and arrange them such that they help us to discuss the arrival and departure times of given frequencies. The comparison of these gives us a method for determining the phase velocity $c(f)$ along the wave path.

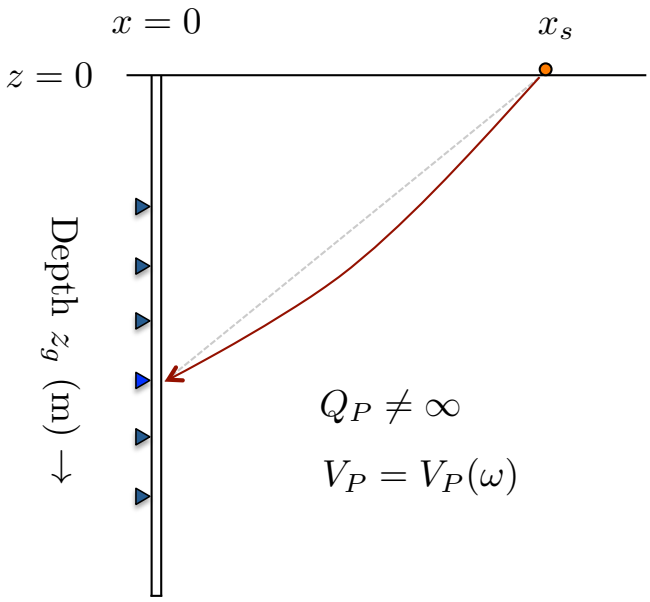

FIG. 1. VSP configuration considered in this paper. The average influence of Q_P and $V_P(\omega)$ over a wave path will be considered, so we will assume an effective homogeneous medium lying between the source point $(x_s, 0)$ and the geophone point $(0, z_g)$.

Time of departure of frequency f in a vibroseis sweep

Suppose a vibroseis sweep begins at $t = 0$. A common mathematical model of the sweep program is

$$s(t) = \text{Im}\left[a(t)e^{i\phi(t)}\right], \tag{2}$$

with the role of the amplitude $a(t)$ being primarily to taper early and late times, and the phase having the time dependence of the frequency, $f(t)$, encoded in it:

$$\phi(t) = 2\pi f(t)t. \tag{3}$$

A linear sweep would then have the form

$$f(t) = f_{\text{min}} + \left(\frac{f_{\text{max}} - f_{\text{min}}}{T}\right)t, \tag{4}$$

parameterized by the low frequency limit f_{min}, the high frequency limit f_{min}, and the sweep length T. The inverse of the function $f(t)$ is the time at which frequency f departs into the Earth from the vibe pad. Calling this time $\tau_S(f)$, we have

$$\tau_S(f) = t(f), \tag{5}$$

and so, in the case of the linear sweep in equation (4), frequency f departs along its wave path at time

$$\tau_S(f) = \left(\frac{f - f_{\text{min}}}{f_{\text{max}} - f_{\text{min}}}\right)T \tag{6}$$

relative to the sweep start time $t = 0$.

Propagation time of frequency f in a dispersive Earth volume

Assuming a straight ray path (dashed as opposed to solid line in Figure 1), let the time it takes for the seismic wave at frequency f to propagate to the geophone be $\Delta\tau(f)$, satisfying

$$\Delta\tau^2(f) = \frac{x_s^2 + z_g^2}{c^2(f)}. \tag{7}$$

Formula for data analysis

Let $\tau_M(f)$ be the time at which the frequency f arrives at a particular depth z_g after propagating a distance $L = (x_s^2 + z_g^2)^{1/2}$ through the Earth volume. From equations (6)-(7), we have

$$\tau_M(f) = \tau_S(f) + \frac{L}{c(f)}, \tag{8}$$

which means

$$c(f) = \frac{L}{\tau_M(f) - \tau_S(f)}. \tag{9}$$

Assuming an approximately straight ray path, knowledge of the source offset x_s and the depth z_g of the geophone provide L. If the Gabor transform of the programmed sweep is overlain on that of the measured direct arrival, with its first coherent frequency f_{min} set at $t = 0$, the time difference $\tau_M(f) - \tau_S(f)$ can be picked off by hand or by automated picking at each frequency as suggested in Figure 2. With L and $\tau_M(f) - \tau_S(f)$ determined, equation (9) can be used to find the average dispersive wave velocity $c(f)$ experienced by the wave along the path of length L.

In Figure 2 we have significantly exaggerated the differences between the departure and arrival times of the vibe data. We will continue with this idealization in the next section to carry out a proof of concept synthetic, but we must keep in mind that in field data, the time and spatial scales of the experiment coupled with the parameters of a standard sweep make the time differences $\tau_M(f) - \tau_S(f)$ small compared to the absolute times/frequencies we will see on the Gabor time-frequency plane. This has no effect on the concepts or approach, but only on the challenge of extracting useful signal.

SYNTHETIC TESTING

In this section we assemble the numerical tools needed to provide a proof-of-concept test of the uncorrelated vibe data analysis. The key requirements are (1) an accurate forward modelling tool which can accept any desired sweep input and propagate it through a medium characterized by any desired dispersion model; (2) a robust time-frequency decomposition tool such as the Gabor transform; (3) an automatic arrival time picker.

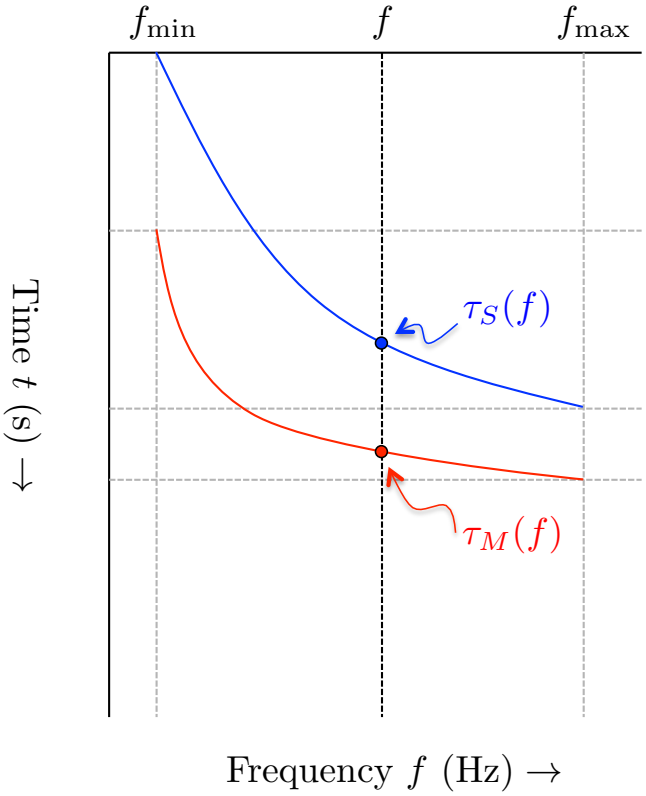

FIG. 2. Scheme for determining $c(f)$ from a comparison of the time-frequency plot of the programmed sweep (blue) compared to the measured uncorrelated sweep (red). The time differences here are exaggerated; in practical applications the difference between red and blue curves on the time-frequency plot would be much subtler.

1D Helmholtz solver with an NCQ wave model

A numerical solver for the 1D Helmholtz equation

$$\left[\frac{d^2}{dx^2} + K^2(x,\omega)\right] P(x,\omega) = 0, \tag{10}$$

where $\omega = 2\pi f$ is the angular frequency, can be used to make the walkaway VSP data set we are interested in analyzing. Although a walkaway VSP problem is fundamentally multidimensional, we are going to study the data assuming simple effective medium along the ray path between the source and receiver. Our interest is also purely in the phase information in the data, so the lack of geometric spreading does not impact the results. In Figures 3a–b a finite difference solution in a two-interface model is shown with the interfaces in red. The propagation constant is chosen to have the NCQ form (Aki and Richards, 2002)

$$K(x,\omega) = \frac{\omega}{c(x)}\left[1 + \frac{i}{2Q(x)} - \frac{1}{\pi Q(x)}\left(\frac{\omega}{\omega_0}\right)\right], \tag{11}$$

which causes the decay and spreading of the pulse when inverse Fourier transformed to $P(x,t)$ as seen in the Figures.

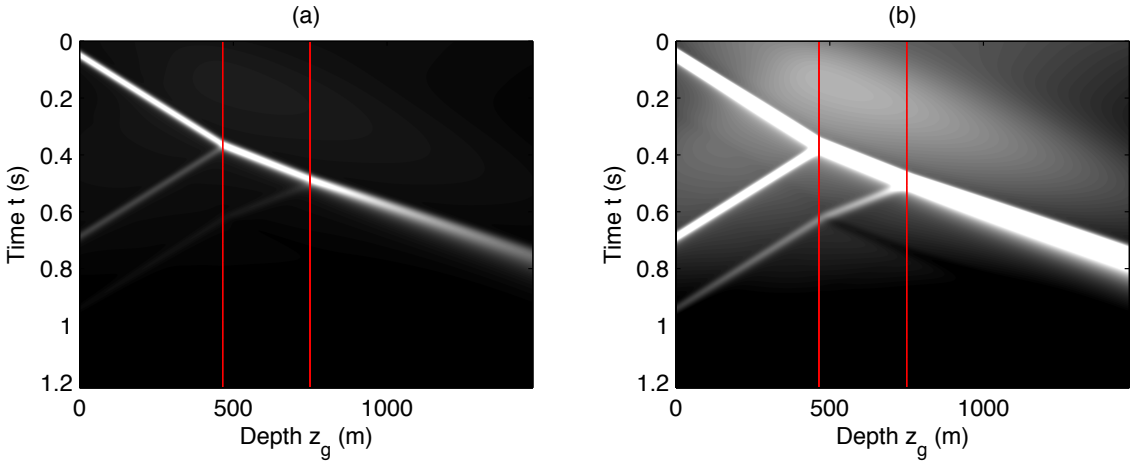

FIG. 3. Helmholtz solution transformed to the physical domain $P(x,t)$. The velocities of the three layers are from top to bottom 1500ms/, 2500ms/ and 3500m/s, and the quality factors of the three layers are 100, 20 and 5. The interfaces are at depths 450m and 750m respectively.

Direct uncorrelated arrivals in walkaway VSP data

In Figures 4a–b the use of the 1D modelled field to simulate reasonably accurate walkaway VSP data is illustrated. The 1D scheme in Figure 4a is solved for a large range of receiver depths (as seen in the example in Figure 3). The desired WVSP data set is put together by matching each one of its source-receiver separations (Figure 4b) to equivalent separations in the 1D data set (Figure 4a). Since we are neglecting amplitudes and spatial variations of parameters in this analysis, this makes for a fast, accurate forward modelling scheme.

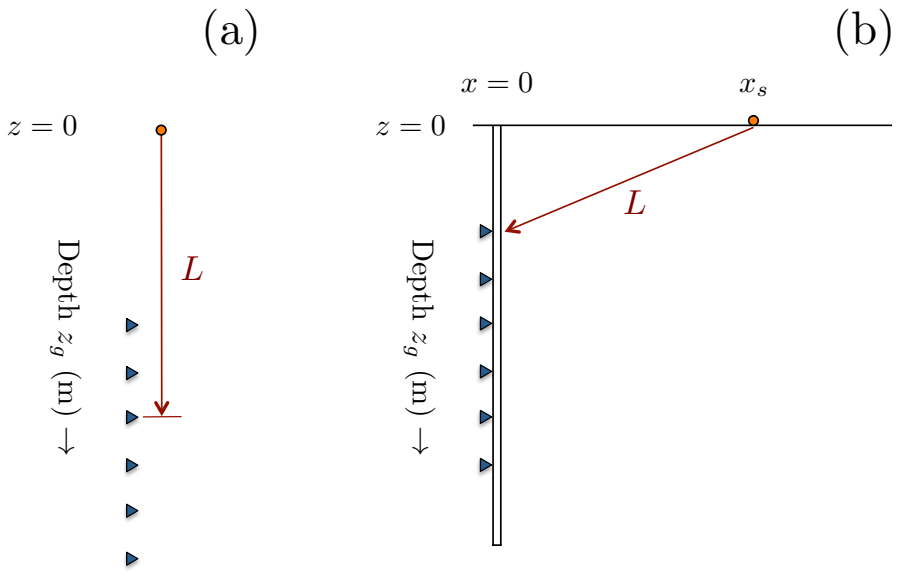

FIG. 4. (a) 1D medium whose traces are calculated with the Helmholtz solver using any desired sweep and any desired dispersion model. (b) The WVSP output configuration. Since our interest is phase analysis assuming homogeneous effective media, we can use traces with the required absolute source-receiver separation from (a) to populate the data set from configuration (b).

A vibe sweep (2-100Hz over 2.5 seconds with 0.15s taper) measured at 40 geophones arrayed between 100m and 4000m depth, from a source 500m offset from the well is synthesized and plotted in Figure 5. The scale of the experiment was deliberately made larger than a standard WVSP, to make our proof-of-concept numerical test a bit easier to carry out and visualize. Nothing in the methodology requires an experiment this large.

Gabor analysis

The CREWES Gabor transform tool *fgabor.m* is used to analyze the traces at each depth of the WVSP data set. In Figure 5 the time-frequency amplitude spectra determined from the geophones at half (a) and three-quarters (b) of the maximum VSP sensor depth are illustrated. The slight $t(f)$ curvature visible in these plots is a consequence of the dispersion of the medium — a linear sweep was input into the medium.

Picking maxima and/or first breaks

The approach is based on the determination of differential times – the times at which a given frequency leaves a source and arrives at a receiver. Whether that differential is measured by picking maxima or first breaks will have to be left until more field data examples have been analyzed and any bias in the Gabor maxima have been identified. In this synthetic study we pick maxima.

In Figures 7a–b the same Gabor spectra illustrated in the previous section are subject to a simple maximum detection routine. These maxima are plotted in yellow. These picks will play the role of the blue curve in the schematic diagram of Figure 2.

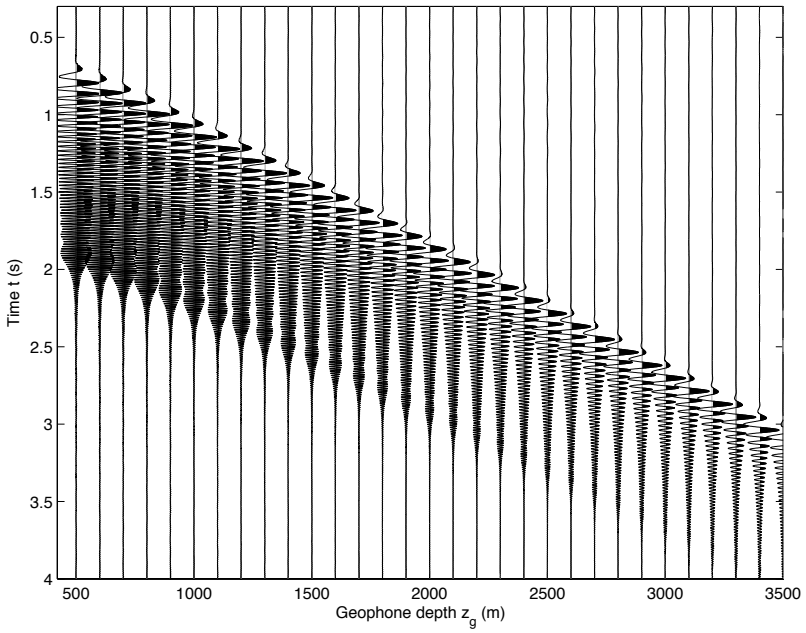

FIG. 5. Synthetic uncorrelated WVSP gather.

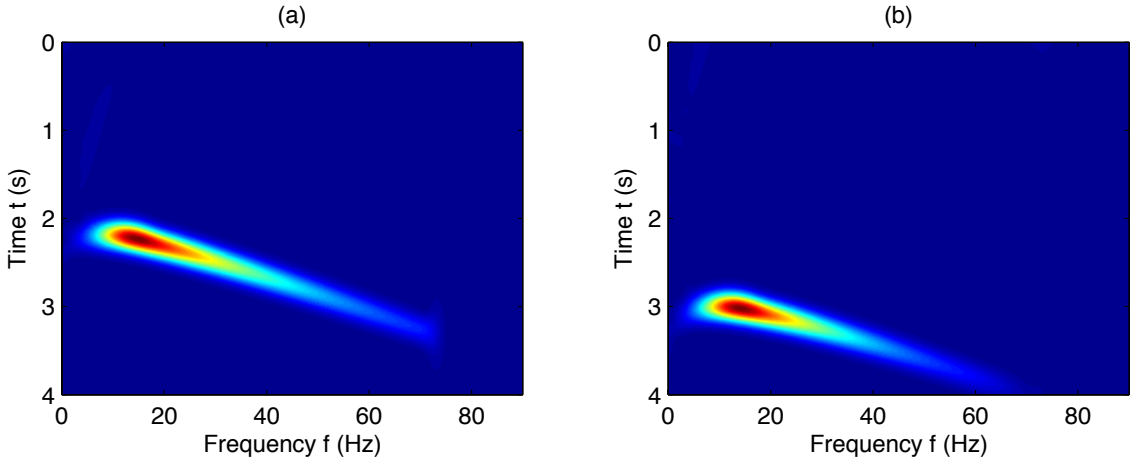

FIG. 6. Time frequency spectra taken from geophones at (a) 1/2 maximum depth and (b) 3/4 maximum depth measuring the uncorrelated sweeps. The slope and curvature of these curves relative to those of the programmed sweeps will drive our $c(f)$ estimation procedure.

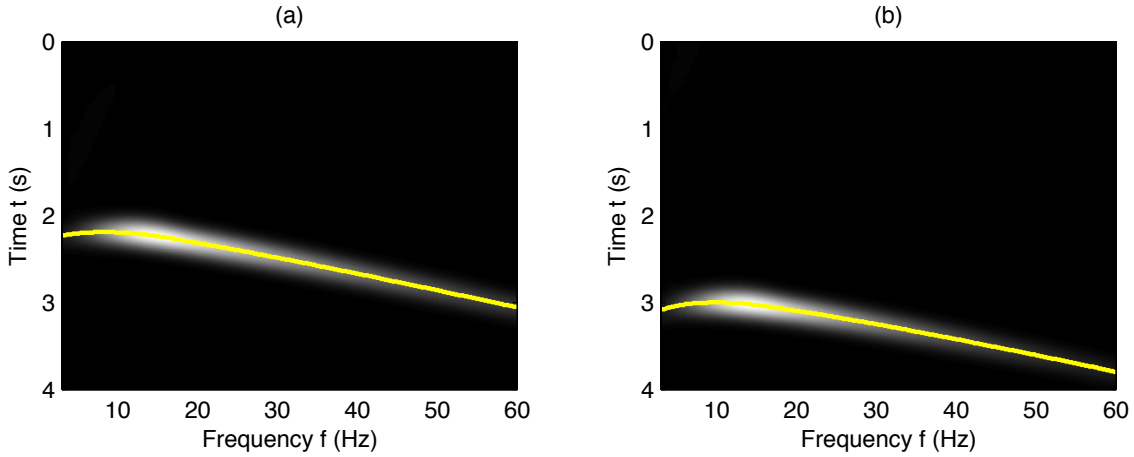

FIG. 7. Maxima picks on Gabor amplitude spectra. Since differential arrival and/or departure/arrival times are the input to the estimation procedure, in principle either maxima or first breaks can be used, provided consistent use of either one is made. Here we use maxima. Whether this introduces any bias or systematic error in the results is a matter of ongoing research. In the field test described in a forthcoming section, we find it more convenient to pick first arrivals of wave energy.

Dispersion estimation

In Figure 8 the original programmed sweep is illustrated. This sweep function is subjected to the Gabor transform, with the starting frequency set at $t = 0$, and the result is plotted on the same t-f plane as the measured sweep.

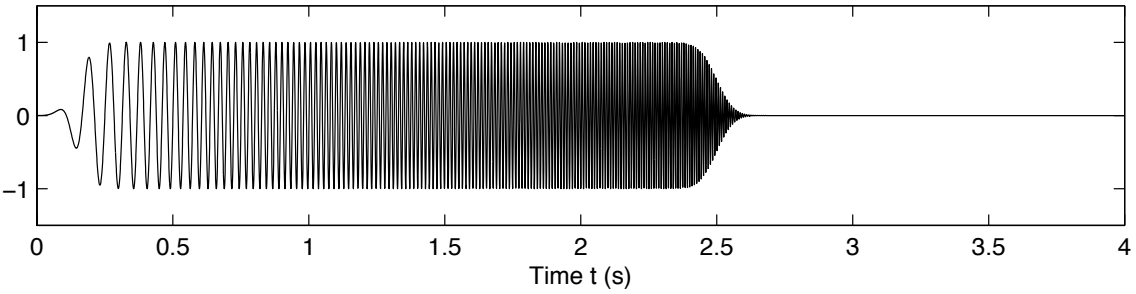

FIG. 8. Programmed sweep $f(t)$. The Gabor transform of this sweep describes a curve which is analyzed as the inverse of the sweep program, $t(f) = \tau_S(f)$, in the time-frequency plane. This provides part of the input for the $c(f)$ calculation.

In Figures 9a-b the amplitude of the programmed sweep is plotted in the Gabor domain with its maxima illustrated in blue. In Figures 9c-d the two measured sweeps (see also Figure 7) after propagation in the dispersive medium are also plotted.

In Figures 10a-b the same plots are repeated with just the picks. At each frequency the difference between the programmed sweep time (in blue, i.e., the time at which that particular frequency left the source) and the measured sweep time (in red, i.e., the time at which that particular frequency arrived at the receiver) is computed. These $\Delta\tau$ values are plotted in Figures 10c-d.

The differences $\Delta\tau$ in Figures 10c-d are used in the denominator of equation (9), with the numerator being estimated from the source and receiver locations and the assumption

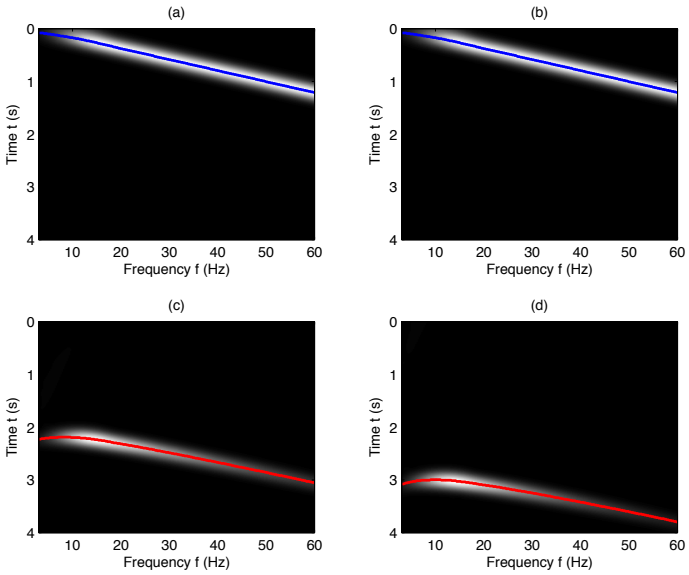

FIG. 9. (a-b) sweep waveform as it departs from the source, with blue curve describing $\tau_S(f)$; (c-d) sweep waveforms as they are measured at two different receiver points, with red curve describing $\tau_M(f)$.

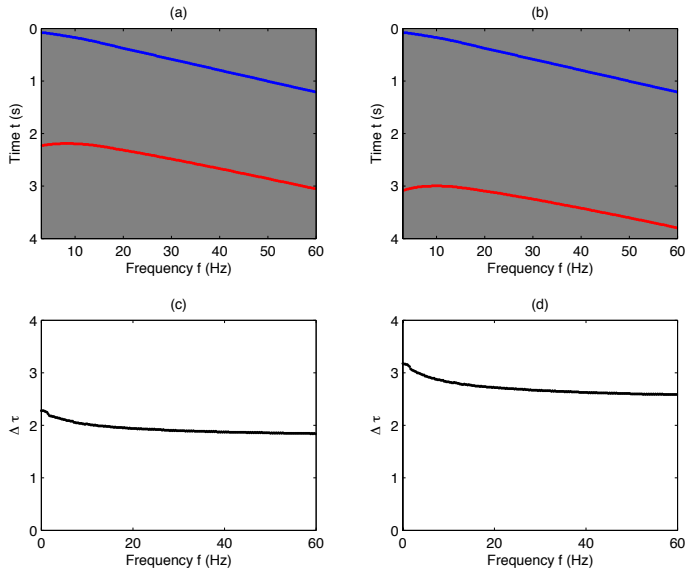

FIG. 10. Repeat of Figure 9 with just the picks represented. The departure/arrival times at each frequency are compared to determine $c(f)$.

of straight ray paths.

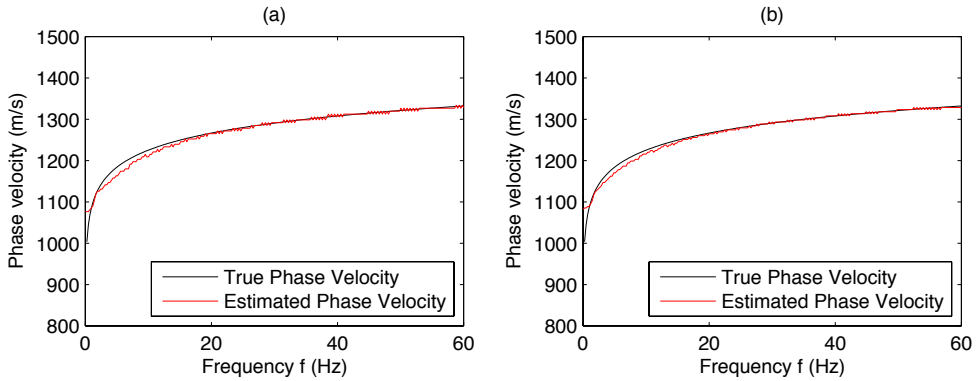

FIG. 11. Estimated phase velocity curves (red) vs. exact phase velocity curves (black). The Q value used in the modelling was 5, and that needed to match the estimated phase velocity was 8 which is likely because of a bias derived from the use of maxima. This may require additional calibration. Nevertheless the trend is matched very well.

Using the time differences read from the Gabor plot and equation (9), we estimate the phase velocity as a function of frequency. The results are illustrated in Figure 11a-b in red overlain on the actual phase velocity curve used in the forward modelling (black), *but* with the latter computed with a slightly higher Q value, 8 instead of 5. We suspect this is indicative of some bias resulting from the use of Gabor maxima. It remains a matter of ongoing study, but our general sense is that we have extracted in a fairly stable manner a good estimate of the phase velocity curve.

FIELD DATA TESTING

Hall et al. (2012) describes a 3C walkaway VSP experiment, in which vibroseis and dynamite sources illuminate 3C geophones arrayed from 60m to 500m depth, in a walkaway mode incorporating offsets from 10m to 1km. The basic configuration of the experiment is illustrated in Figure 12. The figure is somewhat schematic; for greater detail and full discussion of processing see Hall's report.

The v, h_1 and h_2 component geophone responses were transformed into vertical, transverse and radial components after correlation (Figure 13). We will focus on the vertical component in this paper, and make use of the uncorrelated responses.

The sweep program was 10-300Hz over 20s. In Figure 14 the first 5s of the sweep is illustrated, as modelled by the formula

$$s(t) = \text{Im}\left\{a(t)e^{if(t)t}\right\}, \tag{12}$$

where $a(t)$ contains a short taper function (not the taper used in the actual experiment), whose early time effect can be seen between 0 and 500ms on the plot, and where $f(t)$ implements the linear 10-300Hz program.

For our analysis we select a mid-range source offset of 320m. We will extract for initial comparison two vertical geophone responses, one at 120m depth and the other at

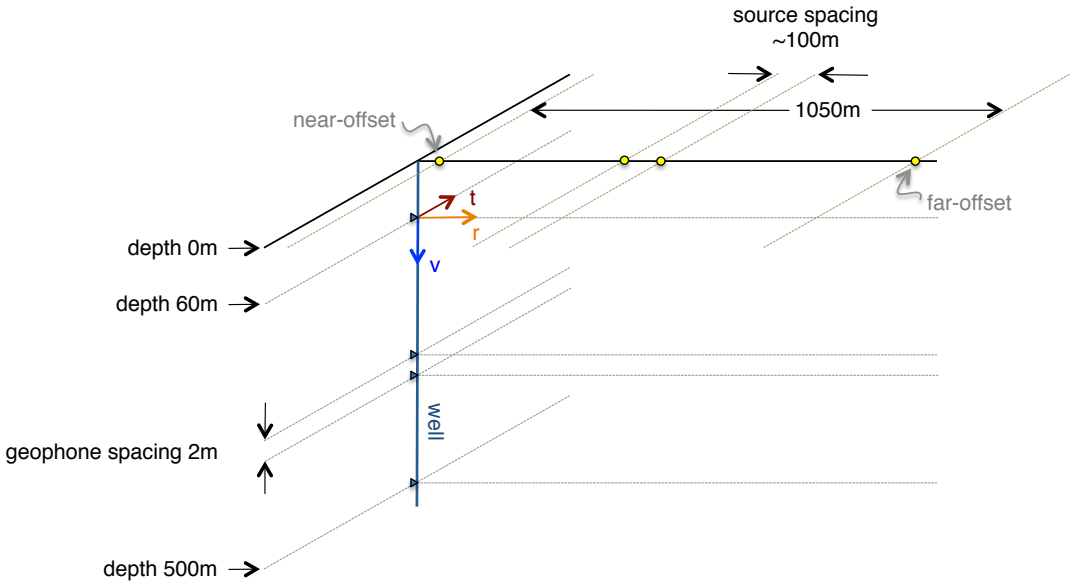

FIG. 12. Configuration of the 3C walkaway VSP experiment. Source points (including vibroseis) are separated by roughly 100m out to a maximum offset of roughly 1km. 3C vectorseis geophones are arrayed at 2m intervals in the well from a depth of 60m to roughly 500m.

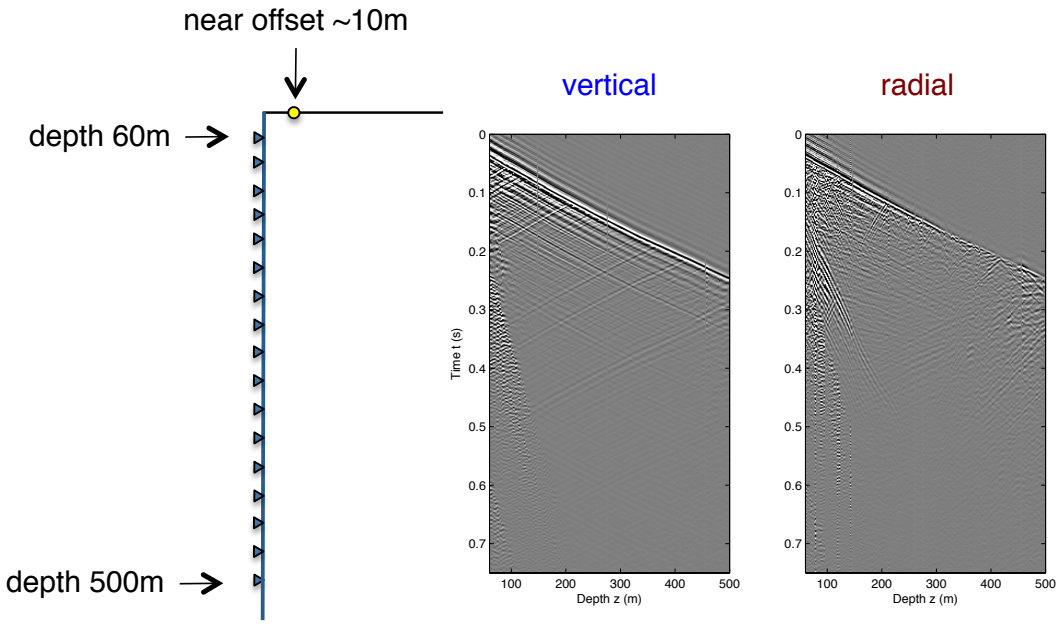

FIG. 13. Correlated data, vertical and radial components, 10m offset (Hall et al., 2012).

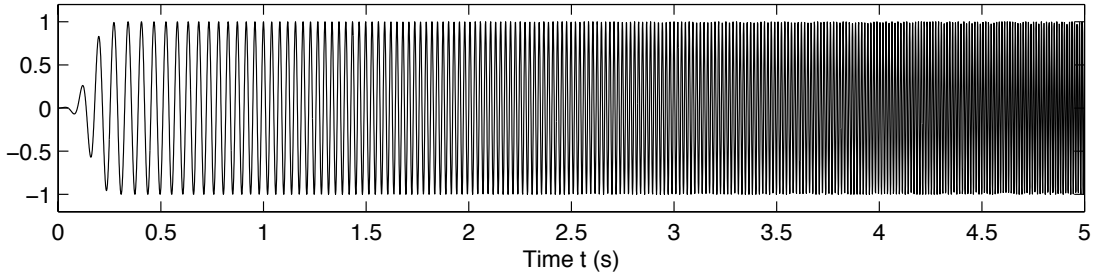

FIG. 14. First 5s of the sweep program, 10-300Hz over 20s (Hall et al., 2012).

400m depth. We aim to strike a balance here: the greater the source-receiver separation, the greater the travel time delay associated with each frequency, and therefore the more pronounced should be our delay signal $\Delta\tau$; however, the greater the separation, the more attenuated the waveform becomes, making discernment of the delay more difficult. With that in mind, in Figure 15 the two extracted traces are plotted near their experimental positions.

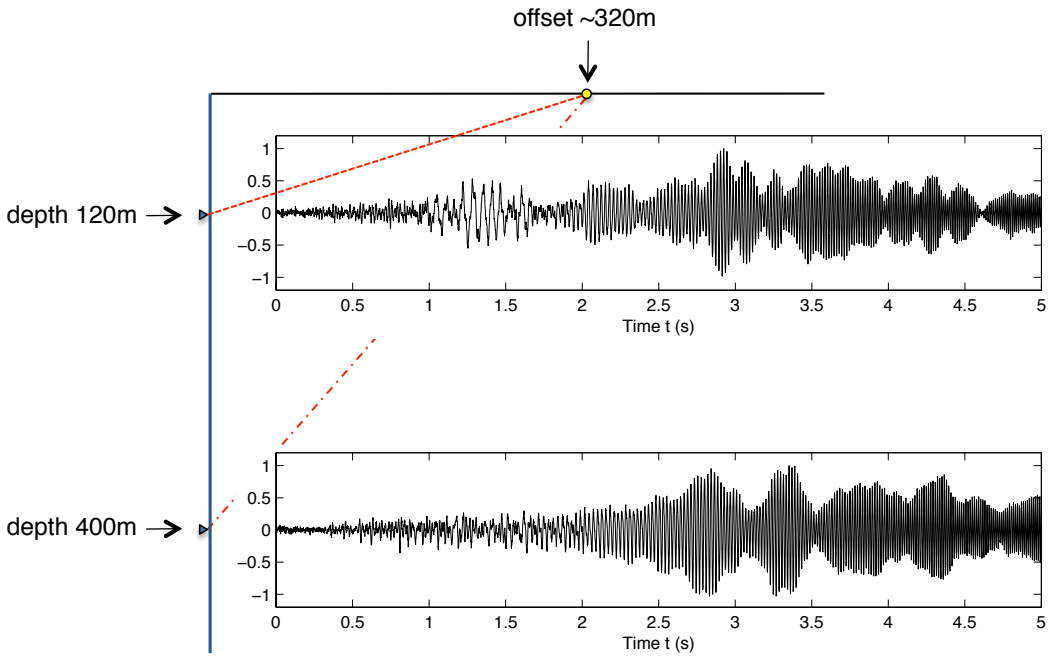

FIG. 15. Uncorrelated vertical component traces are selected from 120m and 500m depth, illuminated from walkaway source at 320m.

The Gabor amplitude spectra of the traces in Figure 15 are plotted in Figure 16, the shallow (a) and the deeper (b). Several harmonics are visible, but the main direct arrival is clearly visible in both panels. The curvature of the arrival time at lower frequencies is more pronounced in the shallower response. The reason for this is likely that the path from the source to the shallower geophone takes the wave through the near surface, which is typically more dispersive than the deeper, more consolidated rock. In any case, we select the Gabor spectrum in Figure 16a to use for our estimation effort.

First breaks in the Gabor spectra of the programmed sweep and the measured sweep

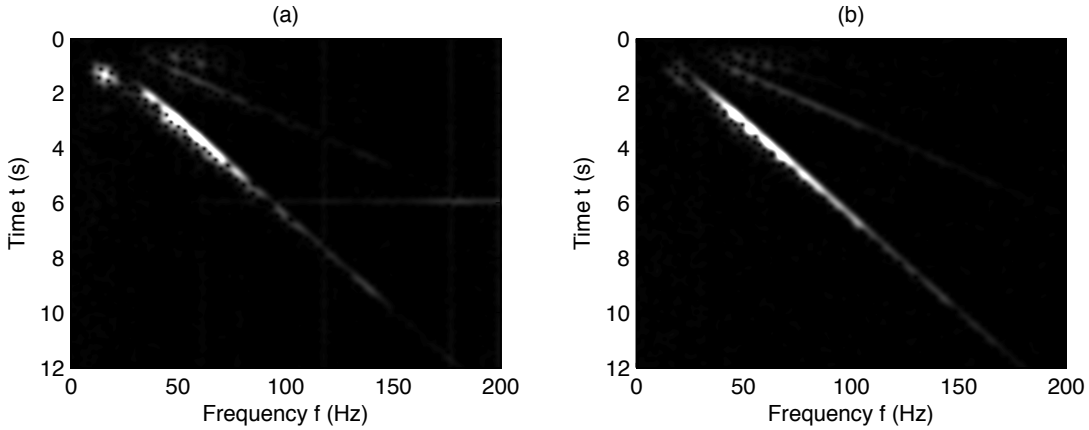

FIG. 16. Gabor amplitude spectra computed from the response of the geophones at (a) 120m and (b) 400m depth. The low-frequency curvature of the direct wave arrival is more pronounced in (a), plausibly because the wave, propagating through a greater part of the near-surface, is subjected to a greater degree of dispersion for a longer duration. We select (a) for our estimation procedure.

are hand-picked (Figure 17), focusing in on the frequency range 10-40Hz.

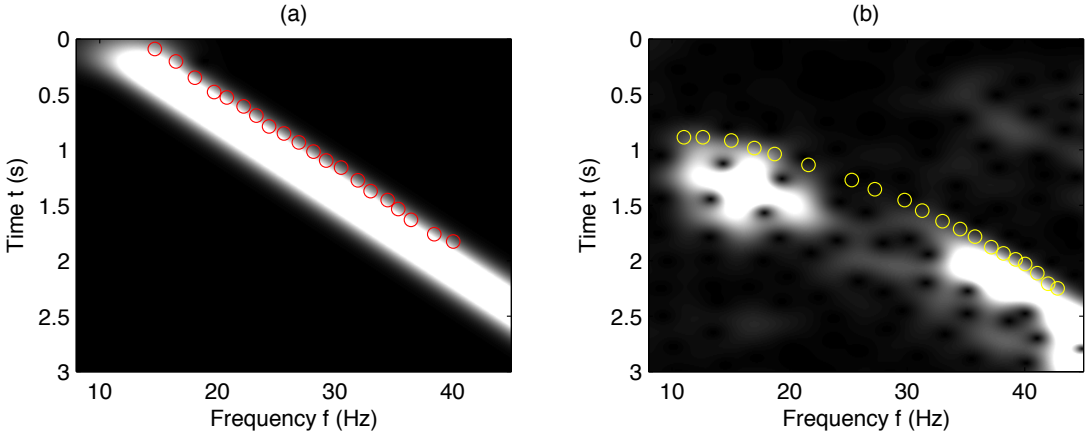

FIG. 17. First breaks on the Gabor spectra. (a) The programmed sweep; (b) the measured direct arrival at the 120m geophone. Frequency range 10-40Hz is focused on.

The picks are plotted together as a function of frequency in Figure 18a, with the programmed sweep in red and the measured geophone response in black. As a validating point, we note that the direct arrivals in Figure 13 have slopes indicative of a velocity of roughly 2000m/s, which means the wavefront moves between the source and receiver in approximately 0.17s. As the slopes of the measured and programmed sweeps come into alignment, beyond 35Hz, the time offset between the (now both approximately linear) sets of picks is close to this value.

The differences $\Delta\tau(f)$ between these two sets of picks are plotted in Figure 18c, and the recovered phase velocities themselves are plotted in Figure 18d. We see a range of velocities between 500m/s at 15Hz to roughly twice that at 28Hz.

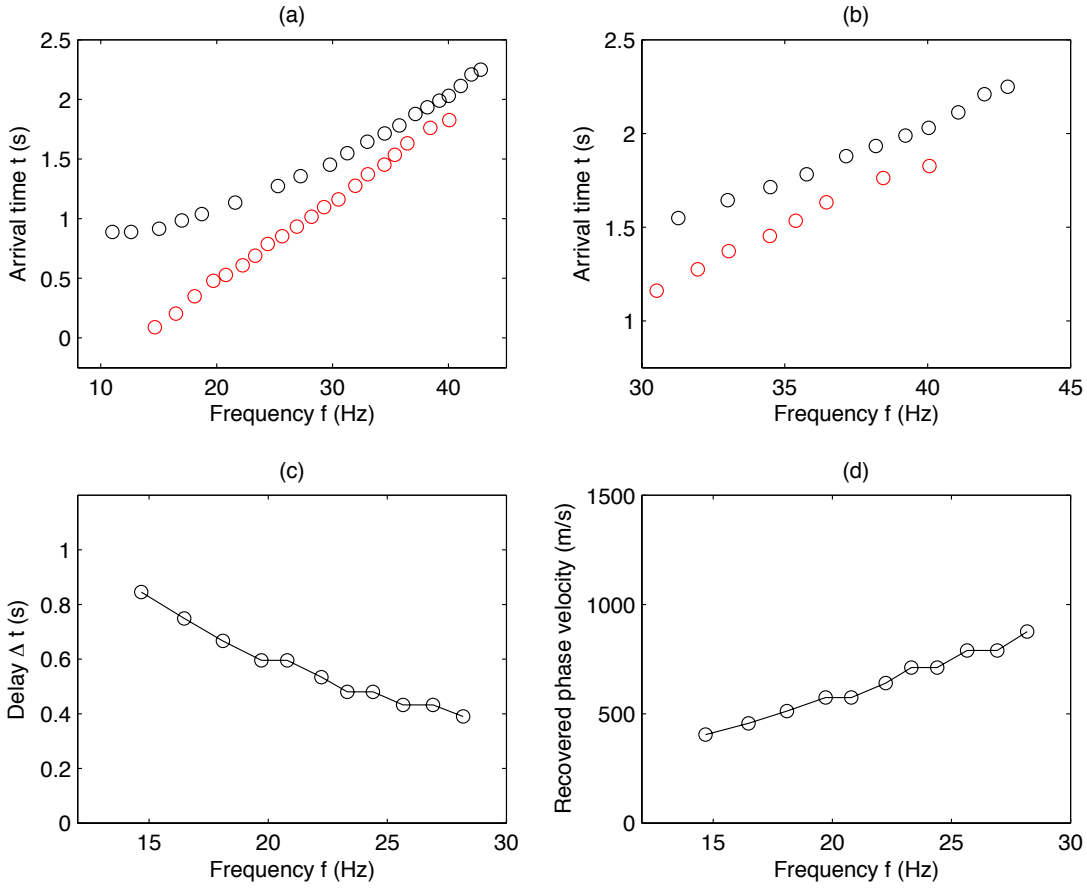

FIG. 18. (a) Programmed sweep arrival time picks (red) vs. measured direct arrival picks (black). (b) The picks form curves with distinct frequency-dependent slopes, but by 35-40Hz the slopes come into approximate alignment, separated by between 0.1s and 0.2s. This agrees with the rough velocity derived from the correlated data. (c) The differential travel times are collected, and (d) transformed via the inversion formula into estimates of the phase velocity curve, which grows from roughly 500m/s at 15Hz to almost 1000m/s at 28Hz.

SELF-CORRELATING EARTH VOLUMES

For every x_s, z_g, and dispersion law $c(f)$, there exists a sweep program for which the Earth volume between the source and receiver brings all frequencies to the measurement point simultaneously. In this situation the measured arrival times $\tau_M(f)$ are all identical, and $\tau_M = \tau_{M_0}$ ceases to be frequency dependent. The delay time at the source is in that case

$$\tau_S(f) = \tau_{M_0} - \frac{L}{c(f)} = \frac{L}{c_0}\left(1 - \frac{c_0}{c(f)}\right) \tag{13}$$

where c_0 is the reference velocity L/τ_{M_0}. Using the fact that $\tau_S(f)$ is the inverse of the programmed sweep $\tau_S(f) = t(f)$ and the program is $f(t)$, equation (13) and a knowledge of the medium dispersion, it is in principle possible to design a sweep which "self-correlates", in the sense that all frequencies will arrive at the geophone simultaneously. Sweeps of this type are likely beyond the specs of most vibroseis sources at the moment, as the frequencies would have to be scanned very rapidly to allow the high frequencies a chance to catch the low.

CONCLUSIONS

A vibroseis sweep and a dispersive geological volume act to negate each other: the sweep delays the arrival of higher frequencies and the dispersive medium hurries them along. We derive a simple analysis procedure in which the time-frequency spectra of a programmed sweep and the uncorrelated measurement are compared in order to estimate the frequency-dependence of the phase velocity. The approach is developed with a synthetic example and applied to the 3C VSP data set. The geophysically reasonable results of this test act as the first validation of the idea.

Further validation of the approach will proceed in two parts. First, the remaining traces and offsets will be subjected to the same analysis. With several 10s, or more, realizations a statistical validation of the estimate will be possible. Secondly, independent Q analysis (Montano et al., 2014) and the assumption of a standard macroscopic dispersion law (e.g., the log of the frequency) can be used as further independent validation. The curve in Figure 18d does not rule out a logarithmic $c(f)$, though to the eye it appears approximately linear in the frequency range we have considered.

ACKNOWLEDGEMENTS

We thank the sponsors of CREWES for continued support. This work was funded by CREWES and NSERC (Natural Science and Engineering Research Council of Canada) through the grant CRDPJ 379744-08.

REFERENCES

Aki, K., and Richards, P. G., 2002, Quantitative Seismology: University Science Books, 2nd edn.

Cheng, P., 2013, Anelastic attenuation in seismic data: modeling, measurement, and correction: Ph.D. thesis, University of Calgary.

Hall, K. W., Lawton, D. C., Holloway, D. E., and Gallant, E. V., 2012, Husky 2011 walkaway 3C-VSP: CREWES Annual Reports, **24**.

Margrave, G. F., 1998, Theory of nonstationary linear filtering in the Fourier domain with application to time-variant filtering: Geophysics, **63**, 244–259.

Margrave, G. F., and Lamoureux, M., 2001, Gabor deconvolution: CREWES Annual Reports, **13**.

Montano, M. C., Lawton, D. C., and Margrave, G. F., 2014, Shallow Q_P and Q_S estimation from multicomponent VSP data: CREWES Annual Reports, **26**.

Tonn, R., 1991, The determination of the seismic quality factor Q from VSP data: a comparison of different computational methods: Geophysical Prospecting, **39**, 1–27.

Zhang, C., and Ulrych, T. J., 2002, Estimation of quality factors from CMP records: Geophysics, **67**, No. 5, 1542–1547.